Geophysical signatures of mineral deposit types in Finland
Edited by Meri-Liisa Airo
Geological Survey of Finland, Special Paper 58, 71–88, 2015

PRACTICAL 3D ELECTROMAGNETIC MODELLING AND MAGNETIC SUSCEPTIBILITY EFFECTS - THE CASE OF KELLOJÄRVI, EASTERN FINLAND

by

Ilkka Suppala[1]

Suppala, I. 2015. Practical 3D electromagnetic modelling and magnetic susceptibility effects – the case of Kellojärvi, eastern Finland. *Geological Survey of Finland, Special Paper 58,* 71–88, 10 figures.

This paper discusses the effect of anomalous magnetic susceptibility in frequency-domain airborne electromagnetic (AEM) and ground Slingram measurements of the Geological Survey of Finland (GTK). Numerical modelling using tabular bodies having anomalous electric conductivity and/or magnetic susceptibility demonstrated differences in the response behaviour. A magnetized vertical plate causes a maximum anomaly when the magnetizing field is along the plate. Conductivity causes a maximum anomaly when the transmitted magnetic flux is perpendicular to the plate. The footprints of the EM systems are different in shape and volume for conductivity and susceptibility. Measured total magnetic intensity (TMI) depicts the anomalous magnetic field caused by induced and natural remanent magnetization, whereas the static remanent component has no effect on the susceptibility model inverted from EM data. The combined interpretation of TMI and EM data provides a way to differentiate the contributions of induced and remanent parts in the TMI anomaly field.

Three-dimensional (3D) geophysical modelling is needed to construct realistic 3D earth models that are consistent with the available geological and geophysical data. However, large-scale and accurate numerical 3D EM modelling is a demanding computational problem. Here, the computational efficiency was improved by separating local 3D computational meshes from the 3D earth model. The 3D interpretation model was composed of layers and tabular bodies. The 3D earth model was mapped to a local mesh to obtain an effectively equivalent local simulation mesh where the complex response was calculated for each source point and each frequency. The diffuse EM equations were solved using the finite-volume method, in which the mesh is composed of rectangular cells. The objective was to make the calculations possible on an ordinary PC, but computations could be made significantly faster in a parallel computing environment.

The 3D model-based interpretation process was tested on the Kellojärvi serpentinitic formation, which is known for its high magnetite content. Both conductivity and susceptibility were taken into account in the interpretation of Twin Otter AEM and ground Slingram data. A parametric 3D interpretation model gave an (approximate) outline of the true conductivity and susceptibility structure. The modelled susceptibilities and conductivities were in agreement with petrophysical measurements from drill core samples. In the ultramafic formation, the ratio of

the remanent to the induced magnetization has been estimated to be two or more, which agrees with petrophysical information on the serpentinites in the study area.

Keywords (GeoRef Thesaurus, AGI): geophysical methods, airborne methods, electromagnetic methods, electrical conductivity, magnetic susceptibility, three-dimensional models, ultramafics, serpentinite, Kellojärvi, Finland

[1]*Geological Survey of Finland, P.O. Box 96, 02151 Espoo, Finland*

E-mail: Ilkka.suppala@gtk.fi

INTRODUCTION

Electromagnetic (EM) methods are used for mapping electromagnetic properties of the ground, for locating conductors, and for mapping overburden and the geology and structure of bedrock. The principal task of airborne or ground EM surveys is to delineate the subsurface electrical conductivity (σ), but frequency domain EM methods are also sensitive to anomalous magnetic susceptibility (χ). The effect of dielectric permittivity (ε) is negligible at low frequencies, but a dielectric response may be observable in high-frequency EM data (e.g. using a helicopter-borne EM system; Huang & Fraser 2001). The low altitude airborne EM (AEM) data in Finland measured by the Geological Survey of Finland (GTK) (e.g. Leväniemi et al. 2009) using one, two or four frequencies have primarily been interpreted visually, e.g. using original or transformed EM data, other geophysics, geological information and known the topography.

In many geological studies, the goal is to build a three-dimensional (3D) geological model of the study area. These 3D earth models should be consistent with available geophysical and other information, which means that geophysics should be modelled and inverted as 3D models. To extract geological information from AEM and ground EM surveys on a local scale, it should be possible to simulate the responses with 3D numerical models.

In this paper, I discuss the numerical calculation of the frequency-domain EM responses of GTK's Twin Otter AEM system with vertical coplanar coils (Suppala et al. 2005), and a ground Slingram system with horizontal coils. The 3D ground is assumed to be composed of layers and tabular bodies of varying electromagnetic properties. Accurate numerical 3D EM modelling can be a challenging computational problem. Therefore, in practice a compromise has to be made between accuracy and computational speed in the modelling process. To limit the computer memory requirements and to speed up the computation, Plessix et al. (2007) separated the modelling mesh representing the whole 3D earth from the computational local meshes used in the finite-integration (finite-volume) method. The computational local meshes are composed of rectangular cells that are made to adapt to the source and receiver location and to the frequency. Commer and Newman (2008) used a similar local mesh approach in 3D EM inversion, but they used the finite-difference method for calculations. In this study, the simulations were carried out using the finite-volume method (Haber & Ascher 2001).

The objective of this study was to simulate the effect of anomalous magnetic permeability ($\mu = 1+\chi$) and to interpret magnetic permeability/susceptibility together with electrical conductivity from AEM and Slingram measurements. The Kellojärvi ultramafic unit has been widely investigated in the context of Ni exploration, and there are excellent geophysical datasets for this type of comparison. Huang and Fraser (2001) simultaneously recovered resistivity ($1/\sigma$), magnetic permeability (μ) and dielectric permittivity (ε) from multifrequency AEM data using half-space models. Simultaneous 1D inversion of conductivity and susceptibility has also been demonstrated to work (e.g. Farquharson et al. 2003, Pirttijärvi et al. 2013). Sasaki et al. (2010) presented an inversion algorithm to simultaneously recover multidimensional distributions of resistivity and magnetic susceptibility from various types of loop–loop frequency-domain EM data (e.g. AEM and Slingram). The calculations were carried out in 3D to invert 2D (elongated 3D) models.

GTK's low altitude (nominal survey altitude of 35 m) AEM measurements have been simultaneously performed with total magnetic intensity (TMI) measurements. Likewise, ground Slingram measurements are accompanied by ground TMI measurements. TMI depicts the anomalous magnetic field caused by induced and remanent magnetization. The induced part is caused by the susceptibility of the ground. The effect of remanent magnetization is often unknown due to the lack of petrophysical measurements. Usually, only the effective susceptibility, assuming no remanence exists, has been inverted from the magnetic data.

By comparing the modelled TMI using susceptibility inverted from AEM data and the observed TMI, we were able reveal near-surface formations with remanent magnetization. For example, Tschirhart et al. (2013) have carried out this type of comparison between modelled and measured TMI data. In magnetic modelling, they used the apparent susceptibility (of a half-space) inverted from AEM data. The purpose of their work was to carry out regional–residual separation for magnetic data utilizing regional apparent susceptibility. As the EM primary field is caused by a magnetic

dipole (rather than by the geomagnetic field), the footprint, i.e. the volume from which the measured information comes, is local, and for susceptibility it is smaller for EM measurements than TMI data. Evidently, frequency-domain AEM and TMI measurements complement each other.

Herein, I present some theoretical 3D modelling results to elucidate the effect of magnetization in AEM and Slingram responses. The measured secondary magnetic field was generated by EM induction and induced magnetization caused by the conducting and magnetically permeable ground. Finally, I present results from a simple case study of Kellojärvi near Kuhmo. A model composed of parametrized bodies and layers makes the computations easier and enables a simple model-based interpretation process.

Numerical modelling on the local meshes

In this study, the theoretical effects of anomalous conductivity and magnetic permeability/susceptibility were calculated using EH3D software, which calculates EM fields in the 3D domain (Haber & Ascher 2001). In EH3D, the system of partial differential equations is discretized using a finite-volume scheme on a staggered grid. The sparse linear system of equations for scattered potentials is solved using an iterative solver (a preconditioned Krylov subspace method BiCGStab). The linear system of equations needs to be solved separately for each source point and each frequency. Therefore, an efficient solution strategy is needed (e.g. Um et al. 2013, Yang et al. 2014).

Plessix et al. (2007) presented a practical approach for multisource, multifrequency controlled-source EM modelling which is well adopted in large-scale EM modelling and inversion (e.g. Cox & Zhdanov 2007). They separated the 3D computational meshes used in the calculations for each source point and each frequency from the modelling mesh, which presents the 3D earth model. An optimal local simulation mesh could be constructed taking into account the resolution capability and the volume of influence (the footprint) of the EM system at the used frequency *f*. The local mesh uses fine cells near the transmitter and the receiver, and coarse cells further away. The volume of the mesh should be larger than the footprint. The grid spacing could be determined from skin depths δ [m] using, for instance, 3–5 mesh nodes per skin depth, where skin depth $\delta = \sqrt{(1/(\mu\sigma\pi f))}$ (Plessix et al. 2007, Commer & Newman 2008).

One way to visualize the volume in which the resolution is higher or lower is to view the EM system's 3D sensitivity distributions. The 3D sensitivity to conductivity for the Twin Otter AEM system has been shown by Suppala et al. (2005), who also used it to delineate the size of the footprint of the EM system. Rahmani et al. (2014) showed 3D sensitivities to both conductivity and magnetic permeability/susceptibility for a crosswell EM configuration. Their theoretical results for the "Slingram in whole space" demonstrated that the sensitivity patterns are different for conductivity and magnetic permeability. The relative sensitivity to magnetic permeability is higher close the EM transmitter and receiver and drops off more quickly than the relative sensitivity to conductivity. These results are congruent with calculations performed in this study.

The geological structure, the model of the survey area, is presented as a set of layers and tabular bodies, where the electromagnetic properties σ, χ and ε are constant. The local meshes are slid along the profile and along the model. For each measurement point and frequency, the electromagnetic properties are mapped to the mesh, and the complex response with sensitivities is calculated. The model is presented as 2D polygons on the vertical plane along the horizontal measurement profile. The polygons are extended along the strike direction perpendicularly to that polygon plane. If only one data line is used in the interpretation, the tabular bodies are extended to effectively 2D models. If multiple data profiles are used, the polygons extend to the middle position between adjacent profiles.

The electromagnetic properties of the tabular bodies formed by 2D polygons are mapped to rectangular cells. When the boundary between different materials cuts the cell, the material averaging/mixing rule determines (approximately) the effectively equivalent properties of the cell. The material averaging formula used here is similar to that of Commer and Newman (2008). A simple method to calculate these averaged (upscaled) values is presented by Abubakar et al. (2009) and is outlined in Figure 1. The resulting mixed material

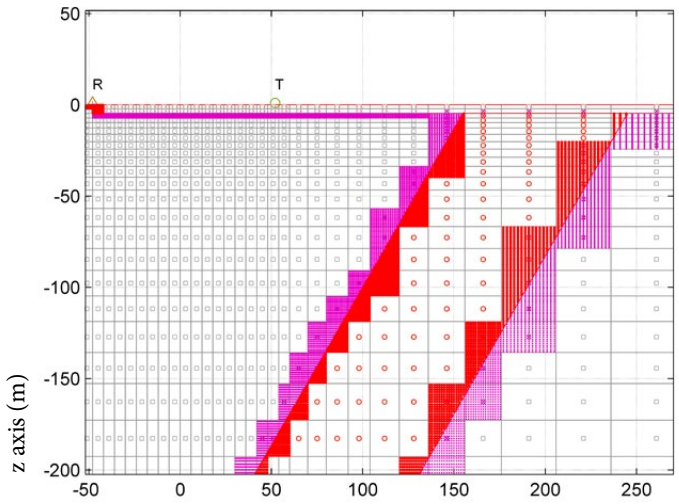

$$\sigma_x(i,j,k) = \left[\sum_{x'}\left(\sum_{z'}\sigma_{x'z'}\right)^{-1}\right]^{-1}$$

The property σ_x of slices perpendicular to the x axis is first calculated as parallel resistors, then the property σ_x of the serial slices.

$$\sigma_z(i,j,k) = \left[\sum_{z'}\left(\sum_{x'}\sigma_{x'z'}\right)^{-1}\right]^{-1}$$

The property σ_z of slices perpendicular to the z axis is first calculated as parallel resistors, then the property σ_z of the serial slices.

Fig. 1. Material averaging of equivalent effective properties for intersected cells with composite materials (Abubakar et al. 2009). The resulting mixed properties σ, χ and ε are anisotropic. The subcells used in the calculation are plotted in small red dots when they are inside the polygons representing a dipping prism and a layer, and in purple when they are outside. The local mesh is used for the Slingram system with a transmitter (T) and receiver (R) coil separation of 100 m and a frequency of 14080 Hz.

properties σ, χ and ε are effectively anisotropic in the scale of the cells. In the EH3D program, σ and ε in these cells are anisotropic and χ is made isotropic, taking the geometric mean of the anisotropic value.

The aim of material averaging is to compute effective material properties on a coarser scale to be used in solving "equivalent" coarse-scale equations. In this study, the used frequencies were relatively low (max 14 kHz), so the diffusive forms of Maxwell's equations were solved. EM systems have a limited resolution (depending on the frequency), which in a sense justifies the approximations explained above. The procedure enables the use of a finite-volume program together with a simple 3D model-based interpretation process.

The matrix of partial derivatives of the system responses with respect to model parameters, i.e., the Jacobian matrix, is calculated as presented by Abubakar et al. (2009). The matrix is computed using the partial derivatives of responses with respect to conductivities of the cells and the partial derivatives of the cell conductivities with respect to the model parameters. The first set of derivatives is calculated by EH3D using an adjoint approach and the second set using effective conductivities (mixing formulas in figure 1) in finite-difference approximations. The method works well with moderate conductivity contrasts that were tested in this study by comparison with finite-difference derivatives (based on changes in the modelled responses due to a slight perturbation of a model parameter). This method is efficient in the calculation of the Jacobian matrix and accurate enough for model-based parametric inversion.

The interpretation of anomalous conductive and magnetically permeable 3D models was carried out here by simple trial-and-error interpretation for one ground profile or flight line at a time, starting with 2D models. So far, model-based optimization using Jacobian matrices has only been tested.

Effect of magnetization in AEM and Slingram responses

The measured quantity of the Twin Otter AEM system and the ground Slingram system is the ratio between the secondary and the primary magnetic fields. The primary magnetic field is produced by a small transmitter coil and could be approximated as a magnetic dipole. The secondary magnetic field is generated by EM induction and induced magnetization caused by the conducting and magnetically permeable ground. The effect of dielectric permittivity ε is negligible at the frequencies used in this study, but in modelling permittivity is also taken into account

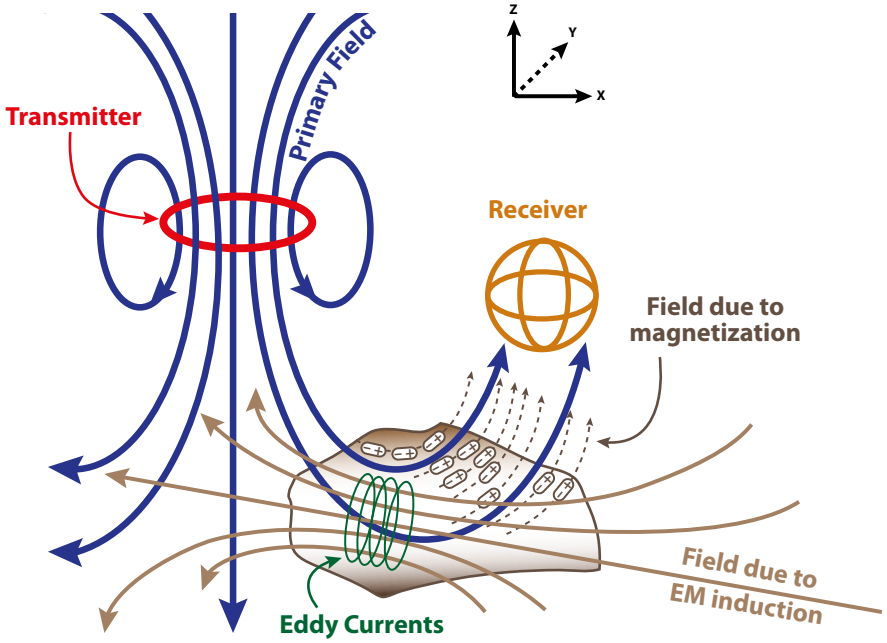

Fig. 2. The principle of EM induction and induced magnetization. The primary field is generated by a transmitter loop or coil. The secondary field is caused by eddy currents and induced magnetization due to the conducting and magnetically permeable subsurface, respectively. (Modified from Grant and West 1965; drawing Harri Kutvonen, GTK).

using some plausible values for water, ice, rock and other media.

The time harmonic primary field induces eddy currents in conductive bodies, which tend to cancel out the changes in the incident primary magnetic field and generate a secondary field. The induced magnetization enhances the internal magnetic field, causing a secondary magnetic field that is in phase with the primary field. This is shown schematically in Figure 2. In the Twin Otter EM system, the conducting ground causes positive in-phase and quadrature responses, while the in-phase component response caused by the magnetically permeable ground has the opposite (negative) sign.

Figure 3 verifies the calculated results by comparing the responses from extensive 3D formations with theoretical 1D solutions. The procedure of local mesh sliding along the profile is used to calculate responses for the Slingram system, where the separation of horizontal loops is 100 m and the frequencies are 3520 and 14080 Hz. Below a 4.7 m thick overburden with a resistivity of 500 Ωm is located a 540 m wide and 800 m long prism in a half-space of 3000 Ωm. The resistivity of the prism is 3000 Ωm or 50 Ωm, and the magnetic susceptibility is 0 or 0.25 [SI]. The height of the prism is 300 m. The 3D model becomes one-dimensional above the centre of the body, when the width of the prism is about 300 m or more. The volumes of the used local meshes were $1100 \times 760 \times 1200$ m^3 and $770 \times 650 \times 920$ m^3 for the frequencies of 3520 and 14080 Hz, respectively. The volumes were discretized into $54 \times 40 \times 42$ and $56 \times 40 \times 38$ cells along x-, y- and z-directions. The minimum cell size was $4.25 \times 4.25 \times 2.2$ m^3 for the frequency of 14080 Hz. The air layer (upper half-space) had a thickness slightly greater than the modelled half-space.

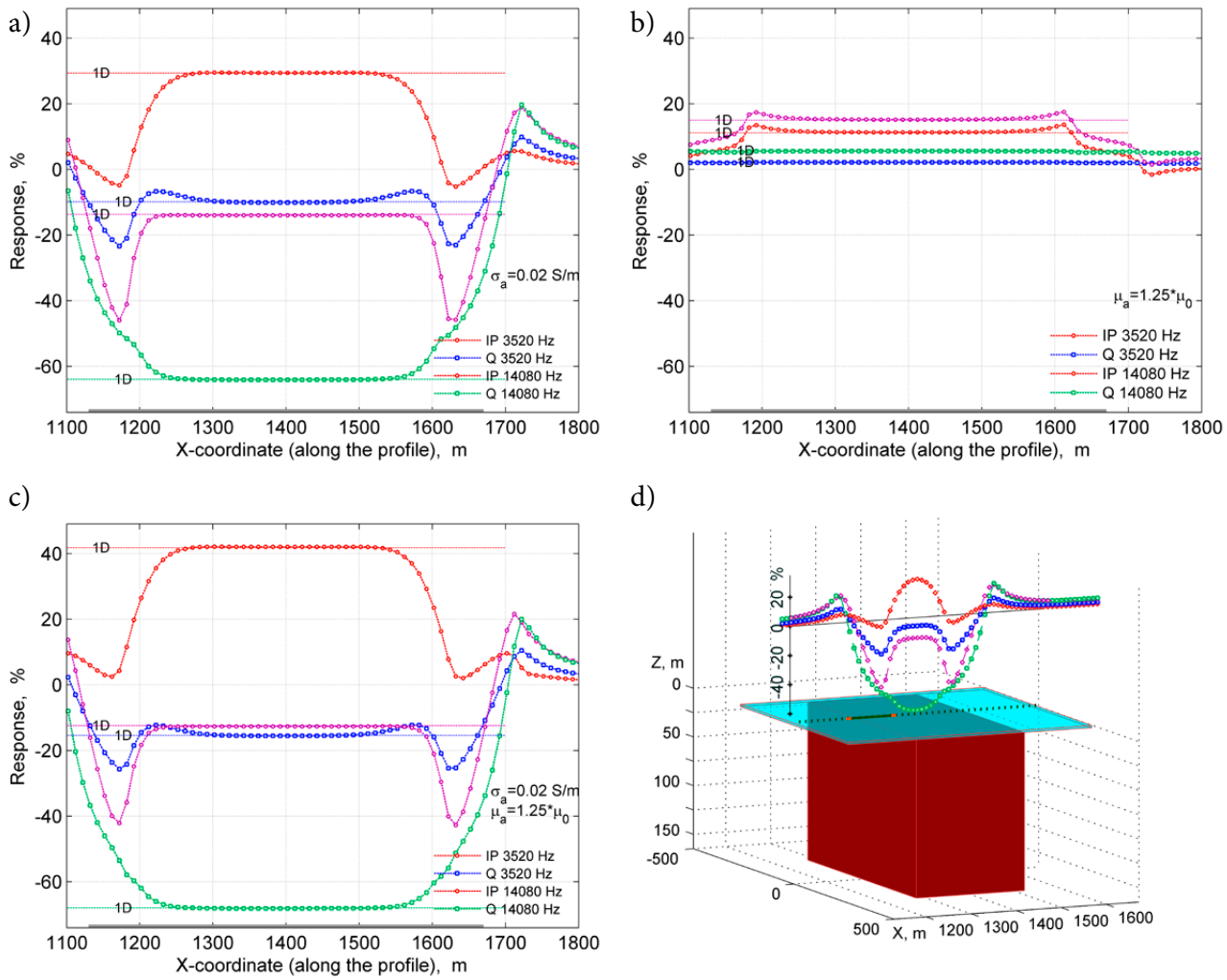

Fig. 3. Slingram profiles (IP = in-phase, Q = quadrature component) over an extensive 3D formation and comparison with 1D results (horizontal lines) at two frequencies (3520 and 14080 Hz). The responses are plotted for a) anomalous conductivity σ, b) anomalous permeability μ and c) anomalous σ and μ. The location of the profile above the 540 m wide prism is indicated in figure 3d.

Figure 4 shows the calculated results for a thinner, 30 m wide, vertical 3D target. Other parameters are the same as those in Figure 3. The magnetized vertical plate causes a maximum anomaly when the receiver or the transmitter is above the plate, i.e. when the magnetizing field is along the plate (Fig. 4b). The conductivity causes a maximum anomaly when the varying transmitted magnetic flux passes through the plate (in Figs 4a and 4c).

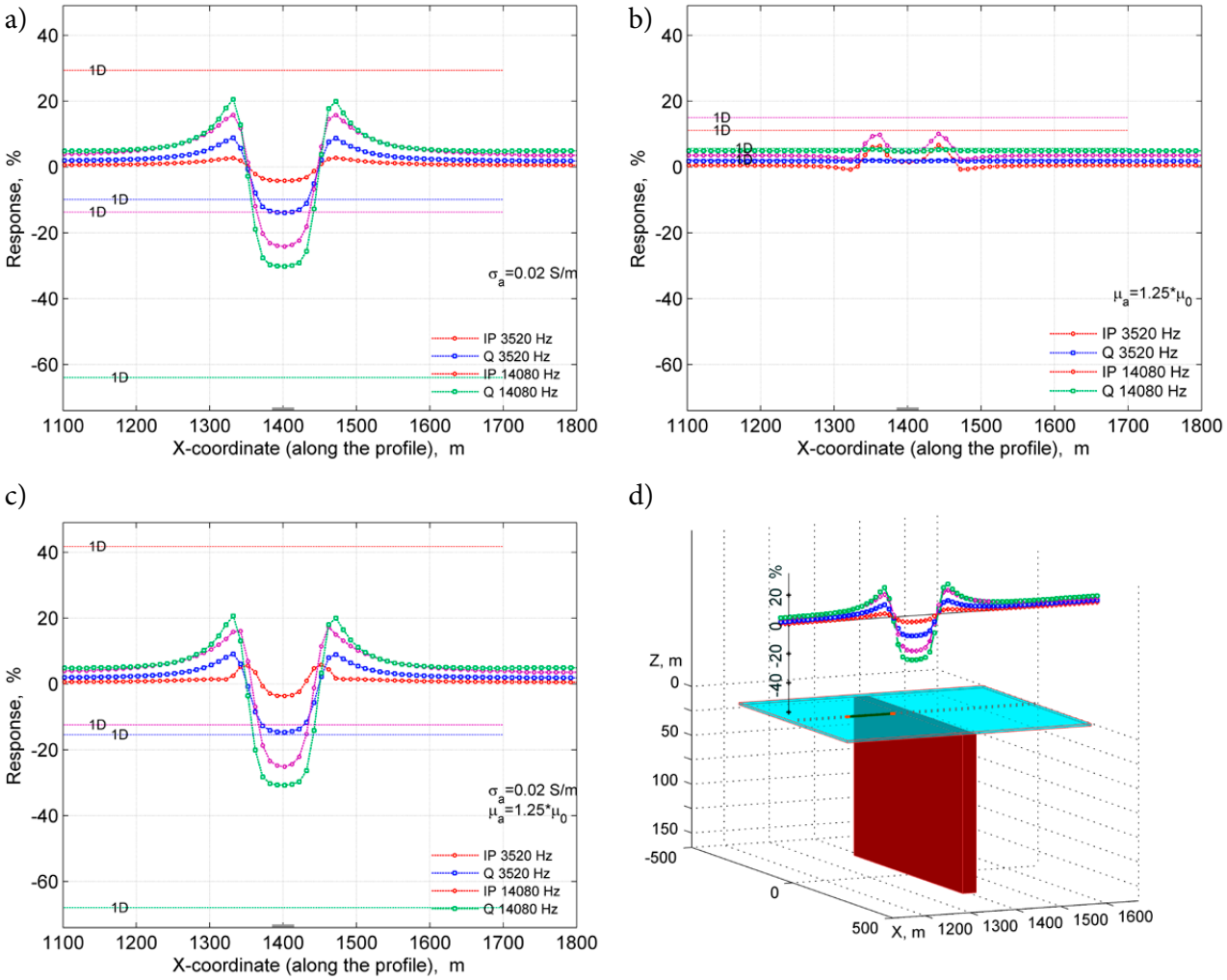

Fig. 4. Slingram profiles (IP = in-phase, Q = quadrature component) over a thin 3D formation and comparison with 1D results (horizontal lines) at two frequencies (3520 and 14080 Hz). The responses are plotted for a) anomalous conductivity σ, b) anomalous permeability μ and c) anomalous σ and μ. The location of the profile above the 30 m wide prism is indicated in Figure 4d.

Figure 5 shows the calculated responses for the GTK Twin Otter AEM system over a thin conductive and/or magnetically permeable vertical prism. The model consists of a vertical rectangular plate with lateral dimensions of 30 m by 270 m, and a vertical height of 254 m. The target is located at a depth of 2.5 m below the overburden within a homogeneous half-space with a resistivity of 3000 Ωm. The resistivity of the overburden is 266 Ωm. The flight lines traverse the centre of the plate, across and along the strike direction. The used frequency was 3113 Hz, and the two flight altitudes were 30 m and 42 m. The volume of the used local mesh was 1190 × 1180 × 1270 m^3. The volume was discretized into 51 × 42 × 45 cells along x-, y- and z-directions. The minimum cell size was 4 × 5.1 × 2.5 m^3. The thickness of the air layer was 730 m.

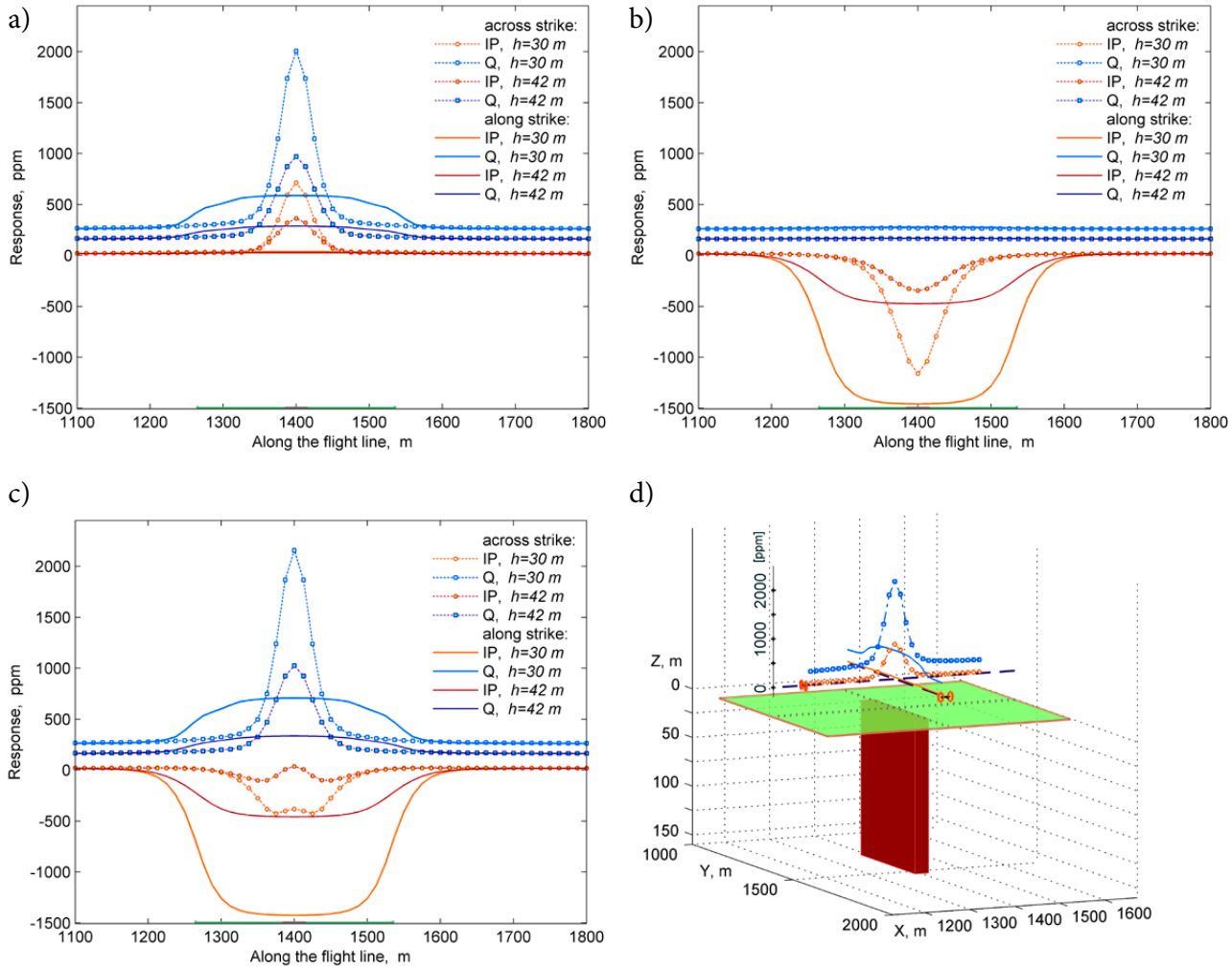

Fig. 5. AEM profiles (IP = in-phase, Q = quadrature component) over the centre of a plate, across and along the strike direction. The responses are plotted for a) anomalous conductivity σ (20 Ωm), b) anomalous permeability μ (1.25*μ_0) and c) for anomalous σ and μ (20 Ωm and 1.25*μ_0). The responses are plotted at two flight altitudes, 30m and 42 m. The locations of the profiles are indicated in Figure 5d.

The results demonstrate the effect of the flight altitude (or the depth of the upper surface of the anomalous body) on the responses. The amplitude of the dipolar primary field as well as the secondary field caused by the anomalous body falls off rapidly ($1/r^3$). All calculated results (see also Rahmani et al. 2014) indicate that the response caused by the magnetization is more sensitive to the distance between the EM system and the target than the response caused by electromagnetic induction by eddy currents.

Calculated synthetic Slingram and AEM responses demonstrate different types of couplings to tabular bodies with anomalous conductivity and/or magnetic susceptibility. The footprints of the Twin Otter EM system are different in shape and volume to conductivity and susceptibility. These theoretical EM results characterize the differences between EM induction and induced magnetization.

On the EM interpretation of conductivity and susceptibility

It is a common situation in geological studies that only incomplete and imprecise geophysical (and geological) data are available. The requirement for the resulting model to be consistent with all available information (as a necessary condition) reduces uncertainty and resolves possible non-uniqueness problems in the interpretation. The ultimate goal should be joint inversion with all

available data and constraining *a priori* information. In this study, the aim was to interpret conductivity and susceptibility from GTK Twin Otter AEM and ground Slingram EM data. Evidently, geophysical magnetic measurements would give mutual and complementary information for the inversion of the susceptibility model.

Magnetic anomalies in TMI measurements are caused by induced magnetization and natural remanent magnetization. The induced magnetization is caused by the susceptibility χ of the ground (multiplied by the inducing magnetic field). The effect of remanent magnetization is caused by permanent static magnetization in ferrimagnetic minerals (e.g. Airo and Säävuori 2013). The static remanent component has no effect on the susceptibility model inverted from AEM data. Calculating TMI values using the inverted susceptibility model and comparing these with the observed TMI values is one method to reveal the near-surface formations with remanent magnetization. Tschirhart et al. (2013) have carried out such work using 1D EM models. This type of cooperative interpretation provides information on the magnitude and direction of remanent magnetization (Clark 2014).

AEM and Slingram surveys use a dipolar inducing field, whereas the geomagnetic field is effectively static and uniform. Therefore, the volume from which the measured information on susceptibility comes is local and smaller in EM surveys than in TMI surveys. In EM surveys, the volume of influence, i.e., the footprint, is clearly shallower. AEM results are more sensitive to the distance from the system to the magnetized target, and are consequently more sensitive to errors in the measured flight altitude. Moreover, the ground magnetic data have better spatial resolution than Slingram in-line measurements made with a wide coil spacing.

Shortening of the transmitter–receiver coil spacing would increase the spatial resolution of Slingram-type EM systems. This would reduce the sensitivity of the EM system to conductivity (operating at a fixed frequency), but not to susceptibility (Won & Huang 2004). Hand-held Slingram-type conductivity meters also operate as susceptibility meters. For example, Wilt et al. (2013) and Rahmani et al. (2014) have examined the possibility to prospect for magnetic targets using a low frequency controlled source in combination with oriented magnetic field receivers. They referred to the method as dipole magnetics or dipole magnetic tomography. Dense measurements with various coil configurations would increase the spatial resolution of susceptibility imaging.

In AEM interpretation, the simplest (and often most practical) model is a 1D layered model of the magnetized and conductive earth. Figure 6 illustrates the sensitivity to the depth to the upper surface of the magnetized basement and the sensitivity to the susceptibility of the basement. The two-layer model has non-magnetized overburden and magnetized basement. The resistivity ρ_1 of the overburden is either 2000 Ωm or 200 Ωm. The thickness of the overburden varies. The resistivity of the basement ρ_2 is 2000 Ωm and its susceptibility χ_2 is 0.1 [SI]. The simulated results are calculated for the two-frequency Twin Otter EM system at the flight altitude of 33 m. Figure 6a shows the change in the AEM response, i.e. the sensitivity, as a function of depth, when the thickness of the overburden increases by one metre. Figure 6b illustrates the change when the susceptibility increases from 0.1 to 0.11 [SI].

In resistive ground, parameters such as the depth to the upper surface of the magnetized body and interpreted susceptibility have a strong (negative) correlation in the in-phase components (e.g. in Fig. 6 when ρ_1 and ρ_2 are 2000 Ωm). The effects of these parameters cannot be interpreted separately (at least by 1D inversion), and one parameter has to be known or predicted to estimate the other. The use of a higher frequency (14 kHz) does not provide any extra information on the magnetized basement (assuming that the possible frequency dependence of the susceptibility is below the noise level), and it does not have a sufficient sensitivity to the thickness of the resistive overburden. When the conductivity of the overburden layer increases to 200 Ωm, the situation is different. Both parameters can be resolved and the information at an additional frequency will benefit in the inversion. This AEM system is also rather insensitive to the thicknesses of the resistive and magnetized formation.

If conventional EM and magnetic survey data are available, the need for joint or combined inversion/interpretation with *in situ* information is emphasized to reduce possible non-uniquenesses in the inversion.

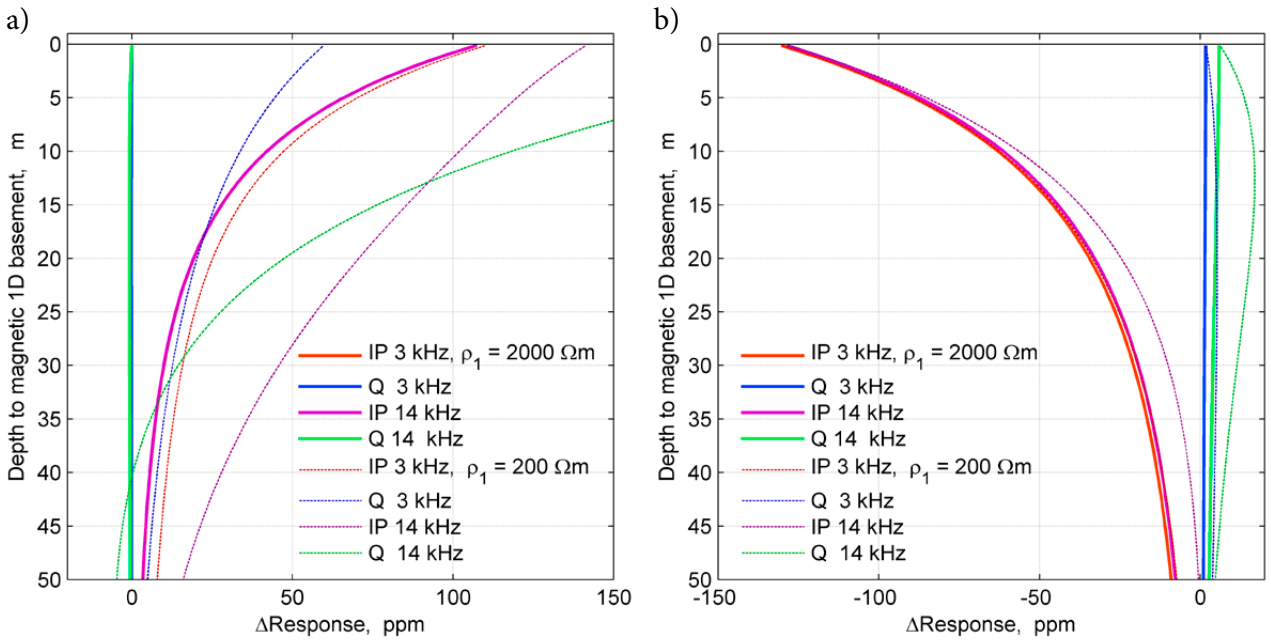

Fig. 6. 1D sensitivities to a magnetic basement below an overburden (ρ_1 = 2000 or 200 Ωm, χ_1 =0.0 [SI], ρ_2 = 2000 Ωm, χ_2 = 0.1 [SI]). Fig. a) illustrates the change in the AEM response as a function of depth if the thickness of the overburden increases by one metre. Fig. b) illustrates the change if the susceptibility increases from 0.1 to 0.11 [SI]. The flight altitude is 33 m.

Kellojärvi interpretation example

2D and 3D model-based interpretation has been tested in the western part of the Kellojärvi ultramafic complex. The area has potential for nickel deposits, and it has been covered by geological and geophysical surveys (e.g. Halkoaho & Niskanen 2012). The area was surveyed in 1994 with 100 m line spacing using a Twin Otter aircraft, simultaneously measuring TMI with two magnetometers, the EM response at 3113 Hz and gamma radiation (Hautaniemi et al. 2005). Large areas have also been covered by ground TMI and Slingram measurements with a line spacing of 50 m. The magnetized ultramafic formation is clearly outlined from aeromagnetic and AEM in-phase data (Fig. 7). The AEM flight profiles and ground profiles are E–W directed. The bedrock is partly outcropping. The topography (Fig. 7a) and bathymetry show rapid topographic variations with clear elongated depressions. The deepest parts of the lake are nearly 20 m deep, while the average depth is less than 10 m.

The bedrock model has been interpreted from the AEM and ground Slingram data using homogeneous 3D σ and χ bodies below Lake Kellojärvi and using estimated overburden resistivity and thickness values. In particular, the lake bathymetry along the measurement profiles has been taken into account. The thickness values for the lake layer are interpolated from the bathymetric elevation model. The 3D models below the profile are extended to the middle position between adjacent profiles, if there is also an interpreted adjacent measurement profile. Otherwise, the model is made infinitely long in that direction. The actual 3D model is comprised of modelled 3D slices, which have a width of about 100 m (AEM) or 50 m (Slingram) and which are wider in the peripheral parts of the modelled area. In principle, all modelled slices are taken into account when the responses along one line are calculated on local meshes, as explained above. In this case study, one "good" local mesh was used per EM system and frequency. Calculated 3D responses caused by wide conductivity and susceptibility formations were tested against 1D results.

The airborne geophysical surveys were conducted in the summer, but the ground geophysics was measured (on the ice) during the winter. The electrical conductivity of the lake water was estimated from AEM results and its dependence on the temperature was taken into account in the Slingram interpretation. The model for the water layer could be more detailed between the flight lines, but this is not a major problem due to the rather high (estimated 240 Ωm) resistivity of the lake water. More

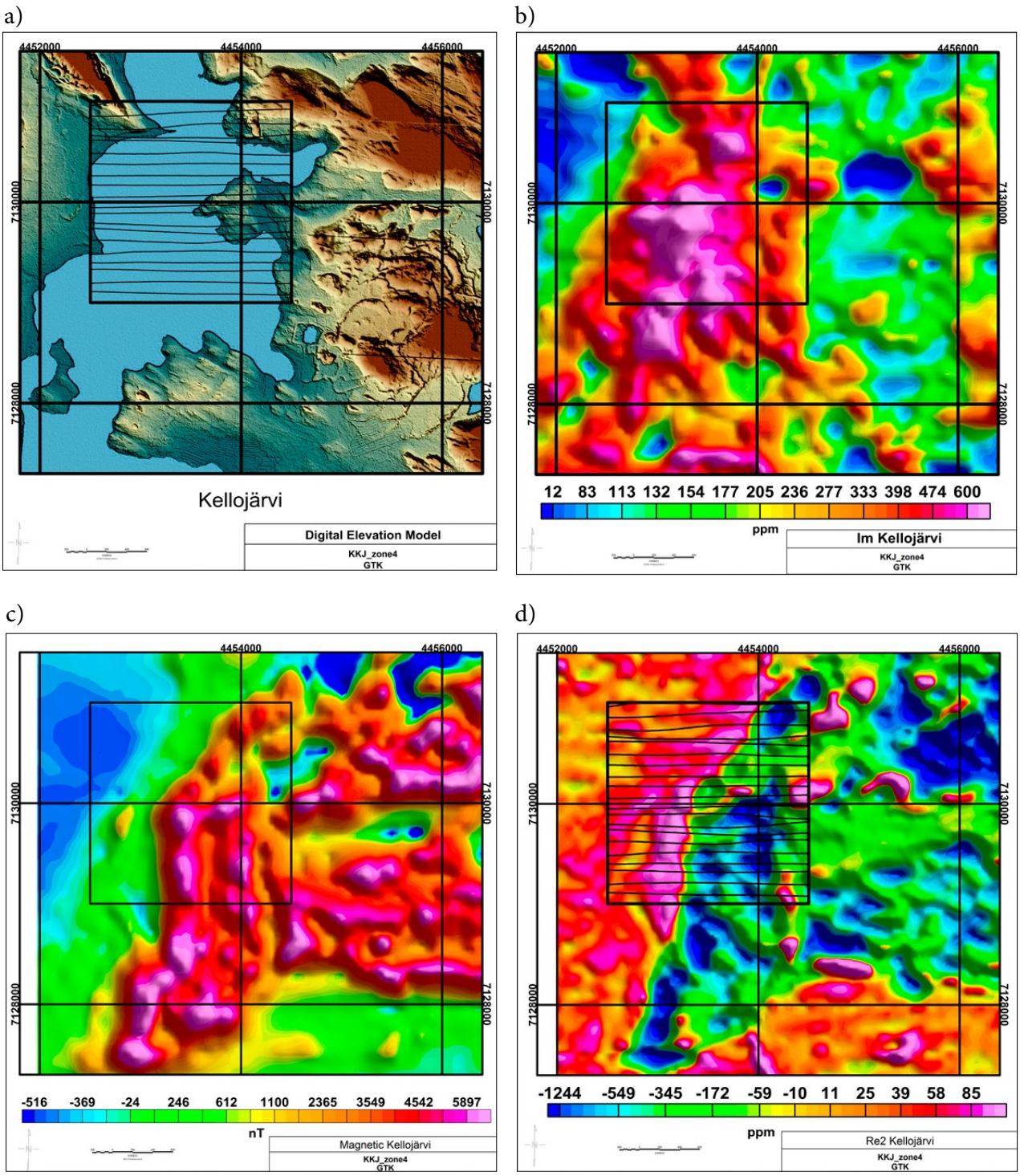

Fig. 7. a) A digital elevation model of the Kellojärvi study area (National Land Survey of Finland) (in the black rectangle, elevation varies from 161 m to 196 m); b) the AEM quadrature component; c) airborne TMI data (IGRF removed); and d) the AEM in-phase component. The black rectangle outlines the study area presented in Figure 10. The AEM flight lines are indicated in Figs a) and d).

care should be taken in estimating the partly outcropping magnetized bedrock formations below abruptly variable topography. Here, the surface topography was assumed to be flat.

In the Twin Otter system, the altitude of the sensors is measured by a radar altimeter. Hautaniemi et al. (2005) estimated that the accuracy of the used radar altimeter is normally better than 0.5 metres. Here, the accuracy of the altitudes was good enough over the lake. Problems arise when the radar altimeter has measured (smoothed) distances to tree tops. Here, the values of the radar

altimeter were (partially) corrected by applying the same type of adaptive (max) filtering as used in Beamish and Leväniemi (2010). The method corrects excessively low altitude values at least to the right direction using measured heights and the digital elevation model. Some more or less erroneous values are nevertheless left, as seen in Figure 8. The high sensitivity of the AEM system to the distance to upper surface of a shallow magnetized body clearly manifests these errors. The (median) filtering of the AEM measurements in the processing step (Hautaniemi et al. 2005) has also caused some minor effects in the AEM responses: the maximum and minimum values have been removed.

Figure 8 displays the AEM interpretation result for flight line 201, which is the nearest to three drill holes shown in Figure 8 c) and d). In this case, a simple visual interpretation of AEM results is also straightforward. In the study area (Fig. 7) there is one evident bedrock conductor; otherwise, the bedrock is resistive. Elongated depressions in topography are related to less resistive bedrock faults/fracture zones cross-cutting the magnetized formation and its surroundings. The westernmost drill hole penetrates into a layer of sulphide-bearing phyllite. The drill core samples give resistivities from few a hundred to 20 Ωm. The easternmost drill hole is in serpentinite, and the middle one penetrates serpentinite at the depth of about 100 m. The measured susceptibilities of the serpentinite are between 0.03–0.22 [SI], and the ratios of the remanent to the induced magnetization, i.e. Q-values, range between 1.2–17, so that there appears to be a positive correlation between susceptibility and remanence.

In this study, the aim was to obtain rough models of conductivity and susceptibility. 3D models give quantitative estimates of model properties. However, these results are still conditional, and the assumptions made should be borne in mind. The usual goodness-of-fit that is attempted to achieve is shown in Figure 8a. As is a common practice in data fitting and inversion, we attempted to find a model for which the modelled and measured data agreed to within noise/error tolerance. In addition, the used parametric tabular 3D bodies may not necessarily explain the measurements more exactly. Thus, the interpretation models give only an outline of the true conductivity and susceptibility models. Twin Otter AEM data are rather insensitive to the dip of the structure. Because the contacts and faults appear to be vertical or subvertical, only vertical tabular bodies were used in interpretation.

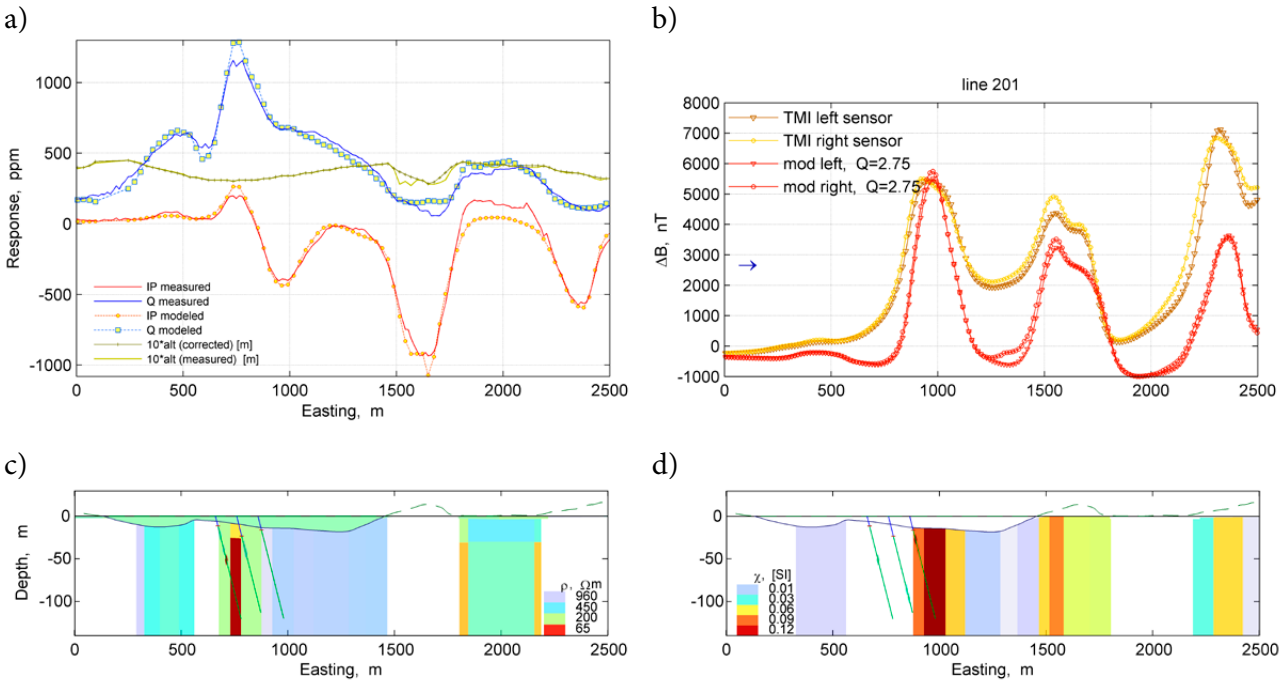

Fig. 8. Interpretation of Kellojärvi AEM data for one profile (201). a) Measured and modelled responses (IP = in-phase, Q = quadrature component) and measured and corrected altitudes; b) measured TMI (IGRF removed) and calculated TMI using the AEM susceptibility model and remanence directed along the geomagnetic field using the Q-value 2.75, with the blue arrow showing the flight direction; c) the resistivity model; d) the susceptibility model. The dashed line in c) and d) indicates the true topography.

The effects of median filtering and errors in the flight altitude can be seen in Figure 8. The variable topography can cause some effects, which were not accounted for in the modelling. The observed in-phase values over a topographic depression (at 2000 m) were not explained well by the model. It is assumedly a fracture zone with increased conductivity, which is more clearly seen in the Slingram results. The values can be explained by a deeper horizontal good conductor. Similar topographic (?) effects can be seen on some other lines.

Comparing the measured TMI values and the modelled TMI response calculated using the interpreted susceptibility model shows a strong effect of the remanent magnetization. In the formation, the ratio of the remanent to the induced magnetization could be 2 or more, which is in agreement with petrophysical measurements from drilled serpentinite in the study area. The modelled susceptibilities are also in agreement, at least qualitatively, with measurements from the drill core samples. Here, the self-demagnetization was not taken into account.

Figure 9 displays the ground Slingram and TMI measurements from profile 7130050, which is closest to the AEM profile line 201. The ground Slingram system is very sensitive to thin vertical conductive structures, which are clearly delineated by the measurements. The dip was also taken into account in the interpretation of the the Slingram data. The (too) fine resolution of the ground TMI is seen over the partly outcropping magnetized formation between Easting 1450 and 1750 m. The small-scale magnetized structures cannot be interpreted from the Slingram data. The topographic variations can cause some error in Slingram measurements.

Figure 10 shows the AEM and Slingram interpretations as maps of vertical cross-sections of conductivity and susceptibility along the measurement profiles. The better resolution of ground Slingram data for vertical conductive structures compared to airborne AEM data is evident. The ground TMI data were partially taken into account in the Slingram susceptibility interpretation. The AEM interpretations were carried out without TMI information to better assess the direction of remanent magnetism. The results in Figure 8c indicate that the remanence could be directed along the geomagnetic field, but there also appears to be another consistent, more westward direction.

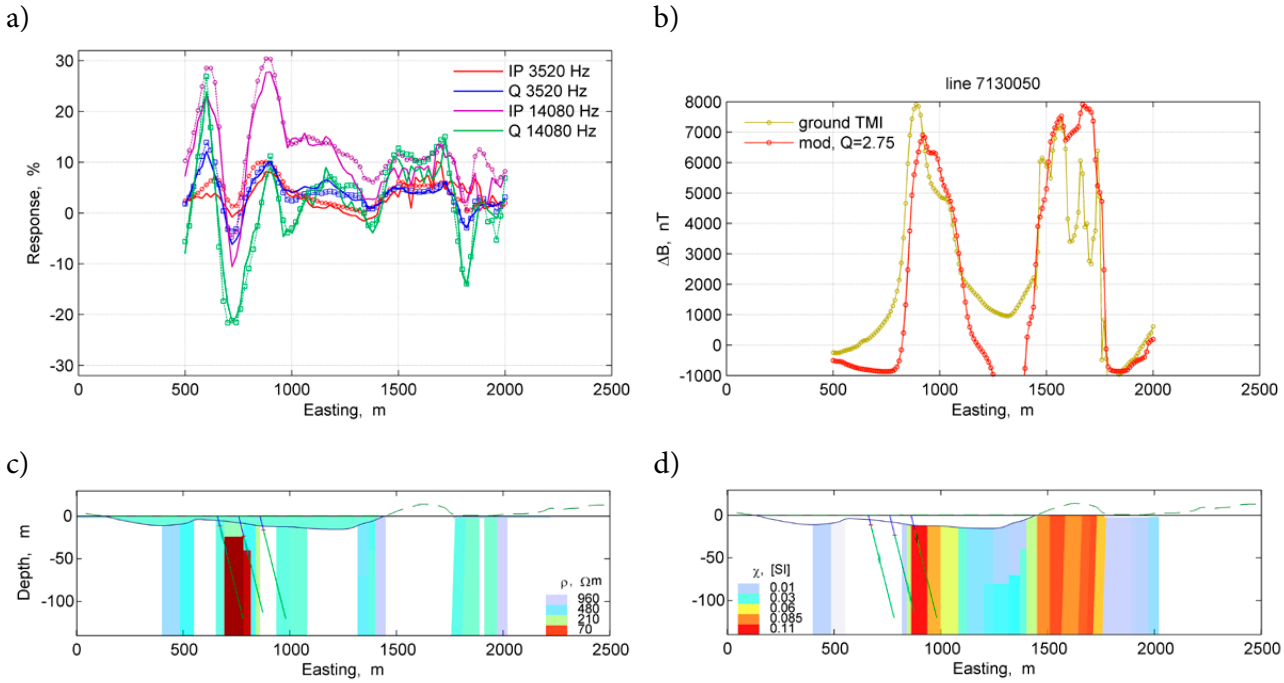

Fig. 9. Interpretation of Kellojärvi Slingram data for one profile (7130050). a) Measured and modelled responses (IP = in-phase, Q = quadrature component); b) measured ground TMI (IGRF removed) and calculated TMI using the EM susceptibility model and remanence directed along the geomagnetic field using the Q-value 2.75; c) the resistivity model; d) the susceptibility model.

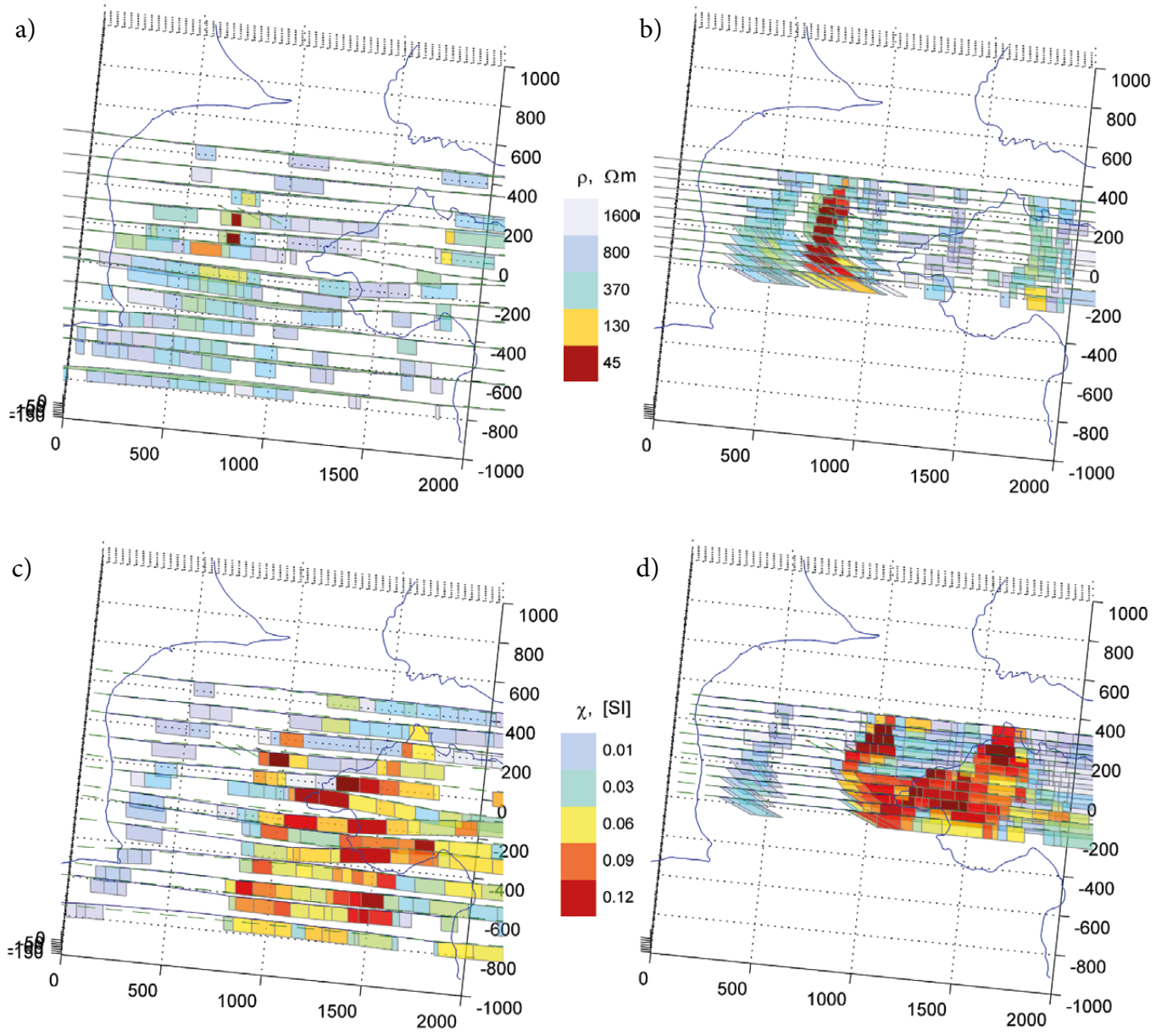

Fig. 10. Interpretation of electrical resistivity (Figs a and b) and susceptibility (Figs c and d) from Kellojärvi AEM (Figs a and c) and Slingram data (Figs b and d). The depth scale in metres of the cross-sections is in the lower-left corner of the maps. The blue lines depict the shoreline of Lake Kellojärvi. Flight line 201 is the nearest to the three drill holes.

CONCLUSIONS

3D geophysical modelling and inversion are needed to construct realistic earth models that are consistent with available geological and geophysical data. Large-scale and accurate numerical 3D EM modelling is a demanding computational problem. A common strategy to improve the computational efficiency is to separate the 3D computational meshes from the 3D earth model and, for instance, from the cell-based inversion mesh. Here, the 3D earth model, i.e. the interpretation model, was composed of layers and tabular bodies with individual electromagnetic properties. A local simulation mesh was used to calculate the complex response for each source point and each frequency. A local simulation mesh was constructed taking into account the resolution capability and the volume of influence (footprint) of the EM system at the used frequency in the local conductivity and magnetic permeability model. The local mesh should use small cells near the transmitter and receiver and coarser cells further away, and the volume of the local mesh should be larger than the volume of influence. The diffuse EM equations were solved using the finite-volume method, in which the local mesh is composed of rectangular cells. This type of approach limits the computer memory requirements. It could also speed up the computations, but above all it makes these calculations possible on an ordinary PC.

In practice, it is required that the 3D model is mapped properly from one presentation to another. Here, the calculated model in the local mesh should be effectively equivalent to the model presented as tabular bodies or as the modelling/inversion mesh. The method to calculate averaged values for a local mesh and to calculate partial derivatives of the system responses with respect to model parameters of tabular bodies is presented by Abubakar et al. (2009). The diffusive nature of the EM fields justifies this scheme for mapping.

Partitioning of the earth by geometric models with individual material properties σ, χ, and ε aids in the use of this finite-volume program and enables a simple 3D model-based interpretation process. The 2D modelling scheme presented by Abubakar et al. (2009) was in this study extended to three dimensions for the EM multiprofile data. The extension is straightforward, and the 3D modelling scheme is workable. For a more detailed model-based inversion, the strike direction could be more carefully taken into account.

The calculated synthetic Slingram and AEM responses demonstrated different types of coupling to tabular bodies that are anomalously electrically conductive and/or magnetically susceptible. Magnetic susceptibility causes a maximum anomaly when the primary magnetic field is parallel to the plate. The conductivity causes a maximum anomaly when the time-varying primary magnetic field (flux) passes through the plate. Simulated results demonstrated that the response caused by magnetization is more sensitive to the distance between the EM system and the target than the response caused by electromagnetic induction by eddy currents. The footprints of EM systems are different in shape and volume for conductivity and susceptibility. These theoretical EM results characterize the difference between EM induction and magnetic induction.

TMI depicts the anomalous magnetic field caused by induced and natural remanent magnetization, whereas a static remanent component has no effect on the susceptibility model inverted from AEM data. The cooperative interpretation of TMI and EM data provides a way to differentiate the contributions of induced and remanent parts in the TMI anomaly field. In magnetic measurements the inducing field is uniform, whereas in Twin Otter and Slingram measurements it is dipolar. Due to the geometrical attenuation of the EM field, the volume of influence is more local and smaller (shallower) in EM surveys than TMI surveys.

The simple 1D layered-earth susceptibility and resistivity interpretation using AEM data alone can be effectively non-unique in resistive environments, when the EM system is not sensitive enough to the conductivity structures. This ambiguity could be resolved using an EM system operating at higher frequencies, measuring densely and with various coil configurations and using 3D interpretation models. The combined inversion of magnetic TMI and EM data would also reduce the non-uniqueness.

The 3D model-based interpretation process was tested in the Kellojärvi case, where both conductivity and susceptibility have been used in the interpretation of Twin Otter AEM and ground Slingram data. The AEM interpretation process is quite straightforward, and here was carried out without

TMI information to better assess the direction of remanent magnetism. The above-mentioned ambiguity is evident in resistive locations. Additional *in situ* information could have been used in the interpretation. For example, the known lake bathymetry was important, and the outcropping magnetized rocks should have been outlined and used in the interpretation with topography. The parametric tabular 3D bodies and layers give a (rough) outline of the true conductivity and susceptibility structure, which was one aim of this work. The modelled susceptibility and conductivity values are in agreement with the measurements from the drill core samples. In the ultramafic formation, the ratio of the remanent to the induced magnetization has been estimated to be 2 or more, which agrees with petrophysics from drilled serpentinite in the study area. The direction of remanence appears to be aligned parallel to the geomagnetic field, at least in some profiles.

The ground Slingram data were found more sensitive to a thin vertical conductivity structure than AEM data. With two-frequency Slingram data, the need for TMI data is more obvious. The future goal is the joint inversion of EM and TMI data using available *a priori* information and constraints.

ACKNOWLEDGEMENTS

I would like to thank Harri Kutvonen, Heli Ojamo and Matti Niskanen for their help and Meri-Liisa Airo for her helpful comments. I also want to thank the reviewers, Markku Pirttijärvi and Ilkka Lahti, for their very constructive reviews.

REFERENCES

Abubakar, A., Habashy, T. M., Li, M. & Liu, J. 2009. Inversion algorithms for large-scale geophysical electromagnetic measurements. Inverse Problems 25, 123012, doi:10.1088/0266-5611/25/12/123012.

Airo, M.-L. & Säävuori, H. 2013. Petrophysical characteristics of Finnish bedrock – Concise handbook on the physical parameters of bedrock. Geological Survey of Finland, Report of Investigation 205, 33 p.

Beamish, D. & Leväniemi, H. 2010. The canopy effect in AEM revisited: investigations using laser and radar altimetry. Near Surface Geophysics 8, 103–115.

Commer, M. & Newman, G. A. 2008. New advances in three-dimensional controlled-source electromagnetic inversion. Geophysical Journal International, 172, 513–535.

Clark, D. A. 2014. Methods for determining remanent and total magnetizations of magnetic sources – a review. Exploration Geophysics 45, 271–304, doi: 10.1071/EG14013.

Cox, L. H. & Zhdanov, M. S. 2007. Large scale 3D inversion of HEM data using a moving footprint. 77th Annual International Meeting, SEG, Expanded Abstracts, 467–470.

Grant, F. S. & West, G. F. 1965. Interpretation theory in applied geophysics. McGraw-Hill. 584 p.

Farquharson, C. G., Oldenburg, D. W. & Routh, P. S. 2003. Simultaneous 1D inversion of loop-loop electromagnetic data for magnetic susceptibility and electrical conductivity. Geophysics, 68(6), 1857–1869, doi: 10.1190/1.1635038.

Haber, E. & Ascher, U. 2001. Fast finite volume simulation of 3D electromagnetic problems with highly discontinuous coefficients: SIAM Journal of Scientific Computations 22, 1943–1961.

Halkoaho, T. & Niskanen, M. 2012. A research report of nickel studies concerning the claim area of Pärsämänsuo 1 (register number of claim: 8344/1) in Kellojärvi, Kuhmo during years 2007–2011. Geological Survey of Finland, archive report 64/2012. 18 p + 29 app. [Electronic resource]. Available at: http://tupa.gtk.fi/raportti/arkisto/64_2012.pdf. (in Finnish)

Hautaniemi, H., Kurimo, M., Multala, J., Leväniemi, H. & Vironmäki, J. 2005. The 'three in one' aerogeophysical concept of GTK in 2004. In: Airo, M.-L. (Ed.), Aerogeophysics in Finland 1972–2004: Methods, System Characteristics and Applications. Geological Survey of Finland, Special Paper 39, 21–74.

Huang, H. & Fraser, D. C. 2001. Mapping of resistivity, susceptibility, and permittivity of the earth using a helicopter-borne electromagnetic system: Geophysics 66(1), 148–157, doi: 10.1190/1.1444889.

Leväniemi, H., Beamish, D., Hautaniemi, H., Kurimo, M., Suppala, I., Vironmäki, J., Cuss, R. J., Lahti, M. & Tartaras, E. 2009. The JAC airborne EM system AEM-05. Journal of Applied Geophysics, 67, 219–233.

Pirttijärvi, M., Abdelzaher, M. & Korja, T. 2013. Fast joint inversion of AEM and static magnetic field data. Geophysical Society of Finland, XXVI Geophysics Days, 97–99.

Plessix, R. E., Darnet, M. & Mulder, W. A. 2007. An approach for 3D multisource multifrequency CSEM modeling: Geophysics 72(5), SM177–SM184, doi: 10.1190/1.2744234.

Rahmani, A. R., Atley, A. E., Chen, J. & Wilt, M. J. 2014. Sensitivity of dipole magnetic tomography to magnetic nanoparticle injectates. Journal of Applied Geophysics 103, 199–214. [Electronic resource]. Available at: http://dx.doi.org/10.1016/j.jappgeo.2014.01.019. Last accessed 17 June 2015.

Sasaki, Y., Kim, J.-H. & Cho, S.-J. 2010. Multidimensional inversion of loop-loop frequency-domain EM data for resistivity and magnetic susceptibility: Geophysics 75(6), F213–F223, doi: 10.1190/1.3503652 .

Suppala, I., Oksama, M. & Hongisto, H. 2005. GTK airborne EM system: characteristics and interpretation guide-

lines. In: Airo, M.-L. (Ed.), Aerogeophysics in Finland 1972–2004: Methods, System Characteristics and Applications. Geological Survey of Finland, Special Paper 39, 103–118.

Tschirhart, P., Morris, B. & Hodges, G. 2013. A new regional/residual separation for magnetic data sets using susceptibility from frequency domain electromagnetic data. Geophysics, 78(6), B351–B359. doi: 10.1190/geo2012-0506.1 .

Um, E. S., Commer, M. & Newman, G. A. 2013. Efficient pre-conditioned iterative solution strategies for the electromagnetic diffusion in the Earth: finite-element frequency-domain approach. Geophysical Journal International 193, 1460–1473, doi: 10.1093/gji/ggt071 .

Wilt, M. J., Chen, J., Alumbaugh, D. L. & Rahmani, A. R. 2013. Dipole magnetics: using low frequency controlled-source EM to map magnetic anomalies. 83nd Annual International Meeting, SEG, Expanded Abstracts, http://dx.doi.org/10.1190/segam2013-0146.1 .

Won, I. J. & Huang, H. 2004, Magnetometers and electromagnetometers. The Leading Edge, 23, 448–451.

Yang, D., Oldenburg, D. W. & Haber, E. 2014. 3-D inversion of airborne electromagnetic data parallelized and accelerated by local mesh and adaptive soundings. Geophysical Journal International, 196, 1492–1507, doi: 10.1093/gji/ggt465 .